ELSEVIER

Biophysical Chemistry 129 (2007) 60–69

Biophysical Chemistry

http://www.elsevier.com/locate/biophyschem

The coordination of protein motors and the kinetic behavior of microtubule — A computational study

Q. Chen [a,*], D.Y. Li [a,b], K. Oiwa [c]

[a] Department of Biomedical Engineering, University of Alberta, Edmonton, Alberta, Canada T6G 2V2
[b] Department of Chemical and Materials Engineering, University of Alberta, Edmonton, Alberta, Canada T6G 2G6
[c] Kansai Advanced Research Center, NICT Biocommunication, Iwaoka, Nishi-ku, Kobe, Hyogo 651-2492, Japan

Received 14 February 2007; received in revised form 9 May 2007; accepted 11 May 2007
Available online 21 May 2007

Abstract

Utilizing the mechanical energy converted from chemical energy through hydrolysis of ATP, motor proteins drive cytoskeleton filaments to move in various biological systems. Recent technological advance has shown the potential of the motor proteins for powering future nano-bio-mechanical systems. In order to effectively use motor proteins as a biological motor, the interaction between the protein motors and bio-filaments needs to be well clarified, since such interaction is largely influenced by many factors, such as the coordination among the motors, their dynamic behavior, physical properties of microtubules, and the viscosity of solution involved, etc. In this study, a two-dimensional model was proposed to simulate the motion of a microtubule driven by protein motors based on a dissipative particle dynamics (DPD) method with attempt to correlate the microtubule's kinetic behavior to the coordination among protein motors.

Keywords: Motor protein; Dissipative particle dynamics; Coordination; Nano-machines

1. Introduction

In recent decades, the rapid development of advanced experimental techniques, such as atomic force microscopy, optical trap nanometry, and fluorescence microscopy, has made it possible to investigate the dynamics of proteins at single-molecule level with different time scales from millisecond to second. The high resolution of the experimental techniques permits probing conformational changes and functions of motor proteins, such as myosins, kinesins and dyneins. These protein-based supramolecular complexes have been extensively studied due to their great potential to act as a biological motor at the molecular scale for nano-bio-mechanical systems or devices. These biological motors can convert chemical energy to mechanical energy through ATP hydrolysis, thus providing power to drive cytoskeletal filaments such as actin filaments and microtubules [1–5]. Efforts have also been made to control the path for these cytoskeletal filaments to move, which makes the development of nano-bio-machines provided by the motor proteins possible. Using a highly oriented polymer film functionalized with myosin subfragments [6] or kinesin [7], the success in driving actin filaments or microtubules in straight lines has been demonstrated. Suzuki and co-workers [8] reported the directional motion of actin filaments driven by aligned and immobilized myosin molecules using microlithographically-patterned resist polymers. In the presence of detergent, kinesin can be selectively attached onto a glass surface, from which the photo-resist polymer has been removed, rather than on the photo-resist polymer itself [9]. The tracks are channels bordered by walls of the resist material, within which microtubules rarely climb up the walls, so that the microtubules can move only along the designed tracks. Controlled movement of microtubules along tracks can also be achieved using micrometer-scaled grooves abricated lithographically on glass surfaces [10,11]. These recent studies have brought the motor proteins closer to bio-engineering applications as a molecular motor. Among different motor proteins, dynein has attracted increasing interest due to the fact that it moves 10 times faster than kinesin [12].

* Corresponding author.
E-mail address: qchen@ualberta.ca (Q. Chen).

0301-4622/$ - see front matter © 2007 Elsevier B.V. All rights reserved.
doi:10.1016/j.bpc.2007.05.008

In order to drive a cytoskeleton filament, motor proteins must grab the filament, hydrolyze ATP and then convert released chemical energy to mechanical energy, thus driving the filament to move. Understanding the mechanism responsible for this energy conversion and driving process is of importance to utilization of motor proteins in future molecular machines. Considerable experimental efforts have been made to investigate relevant issues, including the structure of motor proteins [13–15], elastic behavior of motors and cytoskeletal filaments [16–19], and the motility of motor proteins [20,21], etc. In addition, the rapid progress in the development of advanced experimental techniques, such as atomic force microscopy [22], optical trap nanometry [23] and fluorescence microscopy [24], has provided researchers effective tools to investigate the dynamics of single-molecule in situ with spatial and temporal resolutions down to Å and μs ranges, respectively. This allows direct observation of dynamic processes involving motor proteins, for which macroscopic ensemble-averaged measurements do not work. Two fundamental protein-motor parameters, coupling efficiency and step-size, which can only be indirectly inferred from in vitro motility assays are now accessible using single-molecule techniques that allow direct and simultaneous observation of ATP-turnover and force generation. However, the filament's motion driven by a number of motor proteins is a very complex process, involving ATP hydrolysis, energy conversion, driving and drag actions, which are greatly influenced by the coordination among protein motors. It is not easy to experimentally determine the roles that the individual factors play in the entire process. In order to elucidate experimental observations and understand mechanisms involved, computer modeling has been used to achieve the goal. In 1957, Huxley suggested that a motor protein could be treated as an elastic spring storing mechanical energy and this idea became the basis of a powerstroke model [25]. A swinging lever-arm model, in which the neck region of a myosin consisting of one or more so-called IQ motifs serving as binding sites for calmodulin or calmodulin-like light chains, was proposed [26]. The resultant complex of extended α-helical heavy chain and tightly bound light chains serves as a lever arm to amplify and redirect smaller conformational changes within the myosin motor domain, which occurs when interacts with nucleotide and actin filaments. A so-called biased Brownian ratchet model was proposed to study the action of myosin on actin filament, including directionally biased Brownian motion [27]. A hand-over-hand model was proposed to simulate the walking motion of two-headed kinesin [28]. In the model, two identical motor domains alternatively swing forward at each step while one motor domain remains attached on the track. Further studies suggest that some kinesin molecules exhibit a marked alternation in the dwell times between sequential steps, causing the motors to "limp" along the microtubule. Such type of movement of microtubule suggests an asymmetric hand-over-hand mechanism, called an inchworm mechanism [29], in which one head always leads in the movement. In addition, Qian studied force–velocity relationship and the stochastic stepping of single kinesin based on the theory of Markov processes [30]. Gao et al. proposed a molecular dynamics model based on free energy simulations and experimental binding constant measurements, which makes it possible to develop a kinetic scheme to understand the ATP hydrolysis by F1-ATPase [31].

The previously proposed models are primarily used to explore the driving mechanism for a single motor on a cytoskeleton filament. However, a filament is usually driven by a number of protein motors, which is influenced by many factors, including the density of motors, the coordination among motors that largely affects the driving and drag forces, and the resistance of surrounding liquid to the filament's motion, etc. The existing models are not very suitable for investigating the effects of these factors on the filament's movement.

In recent years, the dissipative particle dynamics (DPD) technique [32] attracted interest due to its large time steps that markedly decrease the computing time so that the powering process of motor proteins involving many factors could be investigated. In 1992, Hoogerbrugge and Koelman proposed a simulation model based on the dissipative particle dynamics (DPD) to study the hydrodynamic behavior of motor proteins [32,33]. In this model, a liquid phase is modeled using dissipative particles and their motion is simulated based on some collision rules. Thermal and hydrodynamic effects could be included in the model, which are of importance to studies on the fluctuation of a microtubule. The DPD method has demonstrated its advantages in simulation of complex fluids and soft materials [34–38]. This method may provide more details of the motor protein's behavior than the stochastic model [30] or the ratchet model [27]. It should be indicated that, compared to the molecular dynamics model such as that used by Gao et al. [31], the DPD model may be limited for qualitative prediction and explanation due to its non-conservation of energy. Since the objective of this study is to improve the understanding of the driving mechanism of dyneins on a microtubule, especially to study the coordination functions of motor protein, rather than quantitative prediction, the DPD appears to be a suitable approach for the present study.

In this study, the authors combined the dissipative particle dynamics (DPD) technique with a bead-and-spring model, and applied the developed method to investigate the motility of a filament driven by motor proteins. Effects of motor density, the coordination among motors, and the microtubule length on the movement of a bio-filament and related issues such as the driving and drag forces were investigated to gain an insight into the interaction between motor proteins and the bio-filament.

2. Model design

2.1. Part A: principles

2.1.1. The DPD simulation method

DPD is a particle-based method [32], in which a fluid is treated as a group of interacting particles. Each particle represents a fluid element containing a number of molecules. The interaction between two particles is a sum of conservative force, dissipative force and random force:

$$F_{\mathrm{is}} = \sum_{j \neq i} \left(F_{ij}^{\mathrm{C}} + F_{ij}^{\mathrm{D}} + F_{ij}^{\mathrm{R}}\right). \quad (1)$$

F_{ij}^{C} is a intermolecular force (conservative), which is a function of the distance between two particles. F_{ij}^{D} is a damping force (dissipative) that is primarily responsible for the viscous effect affected by the relative velocity between a pair of particles. F_{ij}^{R} is a stochastic force caused by the thermal motion of molecules. Since the forces are pairwise, the momentum of the entire system is conserved and its macroscopic behavior directly depends on Navier–Stokes hydrodynamics [32]. The conservative force is expressed:

$$F_{ij}^{C} = \begin{cases} a_{ij}(r_c - r_{ij})\hat{r}_{ij}, & r_{ij} < r_c \\ 0, & r_{ij} \geq r_c \end{cases} \quad (2)$$

where a_{ij} is the maximum repulsive force between particles i and j, which can be determined from the liquid's compressibility; $r_{ij}=|r_i-r_j|$, r_c is a cutoff radius, and $\hat{r}_{ij}$ is the unit vector from particle i to particle j.

For a liquid phase consisting of two different types of particles, A and B, the particle–particle interaction is approximated by letting

$$\begin{aligned} a_{AA} &= a_{BB} = a_0 \\ a_{AB} &= a_0(1+\xi). \end{aligned} \quad (3)$$

A positive ξ results in a larger repulsive force between A and B, while a negative ξ leads to smaller repulsion so that species A and B can be mixed more easily. The value of ξ ranges from -0.5 to 0.5 [35].

The dissipative force and random force can be written as:

$$\begin{aligned} F_{ij}^{D} &= -\gamma w^{D}(r_{ij})(\hat{r}_{ij}\cdot v_{ij})\hat{r}_{ij} \\ F_{ij}^{R} &= \sigma w^{R}(r_{ij})\zeta_{ij}\Delta t^{1/2}\hat{r}_{ij} \end{aligned} \quad (4)$$

$$\sigma^2 = 2\gamma k_B T \quad (5)$$

where σ is the amplitude of noise amplitude, and ζ_{ij} is a random noise term with zero mean and unit variance. γ is a friction coefficient, which is related to σ, as Eq. (5) describes. $\sigma=3$ is recommended based on previous work [39].

It needs to be indicated that F_{ij}^{D} and F_{ij}^{R} are mutually related through w^{D} and w^{R}:

$$w^{D}(r) = [w^{R}(r)]^2 = \begin{cases} (r_c - r)^2, (r \leq r_c) \\ 0, (r > r_c) \end{cases}. \quad (6)$$

For a system in equilibrium, its temperature may be determined from the velocity of particles driven by thermal force:

$$3k_B T = \langle m v^2 \rangle \quad (7)$$

2.1.2. The bead-and-spring model for a polymer chain

In this model, a microtubule is simply treated as a polymer chain. A bead-and-spring chain structure is used. Two adjacent beads are connected by a spring, and the force between neighboring beads i and j is expressed as [40]:

$$F_{ij}^{P} = K(r_{ij} - r_{eq})\hat{r}_{ij} \quad (8)$$

where K is the spring constant and r_{eq} is the stress-free spring length,

For a microtubule, the spring constant of microtubule is expressed as:

$$K = \frac{EA}{L} \quad (9)$$

where E is the elastic modulus of the microtubule, which is determined experimentally, A is the cross-sectional area of the microtubule and L is the length of the microtubule.

In the present study, only unidirectional movement of microtubule was investigated. To simplify the model, the bending strength of microtubule was not taken into account.

2.1.3. The DPD algorithm

Once the force on a liquid particle is given, its velocity and trajectory can be determined using a modified Velocity–Verlet algorithm [41]:

$$\begin{aligned} \vec{r}_i(t+\Delta t) &= \vec{r}_i(t) + \Delta t\cdot\vec{v}_i(t) + \frac{1}{2}(\Delta t)^2\frac{\overrightarrow{f_i}(t)}{m_i}\ \overrightarrow{f_i}(t) \\ \vec{v}_i(t+\Delta t/2) &= \vec{v}_i(t) + \frac{1}{2m_i}\Delta t\cdot\overrightarrow{f_i}(t) \\ \overrightarrow{f_i}(t+\Delta t) &= \overrightarrow{f_i}(\vec{r}_i(t+\Delta t) + \vec{v}_i(t+\Delta t/2)) \\ \vec{v}_i(t+\Delta t) &= \vec{v}_i(t+\Delta t/2) + \frac{1}{2m_i}\Delta t\cdot\overrightarrow{f_i}(t+\Delta t) \end{aligned} \quad (10)$$

where $\vec{r}_i(t)$ and $\vec{r}_i(t+\Delta t)$ are respectively the positions of particle i at time t and time $t+\Delta t$, respectively. $\vec{v}_i(t)$, $\vec{v}_i(t+\Delta t/2)$, and $\vec{v}_i(t+\Delta t)$ are the velocity of the particle at t, $t+\Delta t/2$ and $t+\Delta t$, respectively. $\overrightarrow{f_t}(t)$ and $\overrightarrow{f_i}(t+\Delta t)$ are respectively the total forces on the particle at t and $t+\Delta t$.

2.2. Part B: model design

A microtubule shows polymorphism: the variation in the number of protofilaments. In experimental conditions, it usually contains microtubules having 14 protofilaments or 13 protofilaments. In order to simplify the model, a microtubule with 13 protofilaments was used.

A microtubule with 13 protofilaments is composed of three-start helices of monomer [42], as Fig. 1 (a) illustrates. The diameter of its cross-section is about 25 nm. To simplify the

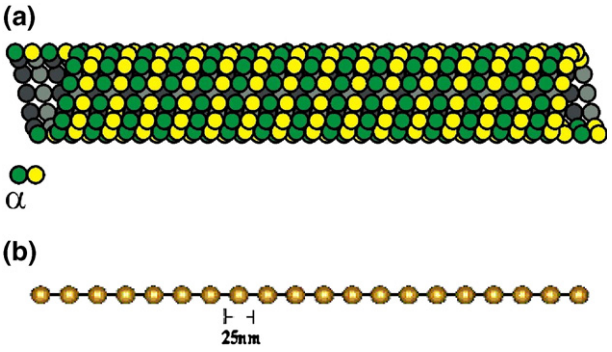

Fig. 1. Structure of a microtubule: (a) a three-start helices structure, (b) a polymer chain structure used to model a microtubule.

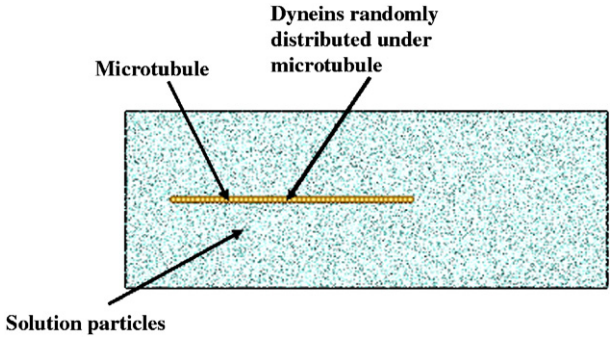

Fig. 2. Sketch of a model system.

model, we treated a microtubule as a polymer chain consisting of springs and beads. A segment of microtubule of 25 nm long was treated as a unit bead, as illustrated in Fig. 1 (b). Since this study focus on the longitudinal movement of microtubule, only longitudinal stiffness of microtubule was taken into account. In this study, the solution in which a microtubule moves is water.

Dimensionless simulation was conducted in the study. We set $\widehat{m} = \widehat{r}_c = \widehat{T} = 1$, where $\widehat{m}$ is the dimensionless mass of a solution particle, $\widehat{r}_c$ is the dimensionless diameter of a solution particle at $r_c = 100$ nm, and $\widehat{T}$ the corresponding dimensionless temperature at $T = 298$ K. According to previous work [43], $a_{ij} = 75k_BT/\rho$ is chosen for water, in which ρ is a number density. In addition, $\rho \geq 3$, $\sigma = 3$ and time step $\Delta t = 0.04$ turn out to be adequate choices. Therefore, $\rho = 3$, $\sigma = 3$ and $\Delta t = 0.04$ were adopted in the present study.

The vertical dimension of the system for this study was set as 40 (Fig. 2). Since different lengths of microtubule were used in the modeling, the horizontal dimension was set to be as twice as that of the longest microtubule. Period boundary condition was applied to both vertical and horizontal dimensions.

According to the power stroke model [25], a motor protein was treated as a strained elastic string after receiving energy from ATP hydrolysis. The strained spring generated a driving force for a microtubule to which it attached. When attached to the microtubule, the strain spring energy was released and thus drove the microtubule to move. For a single motor of dynein c, each power-stroke resulted in a displacement of about 8 nm as determined experimentally [44].

Hence, for each stroke, the driving force of a motor on a microtubule may be expressed as:

$$F_d = k \cdot \Delta\delta \tag{11}$$

where k is the spring constant of the motor and $\Delta\delta$ is the stroke distance of dynein c.

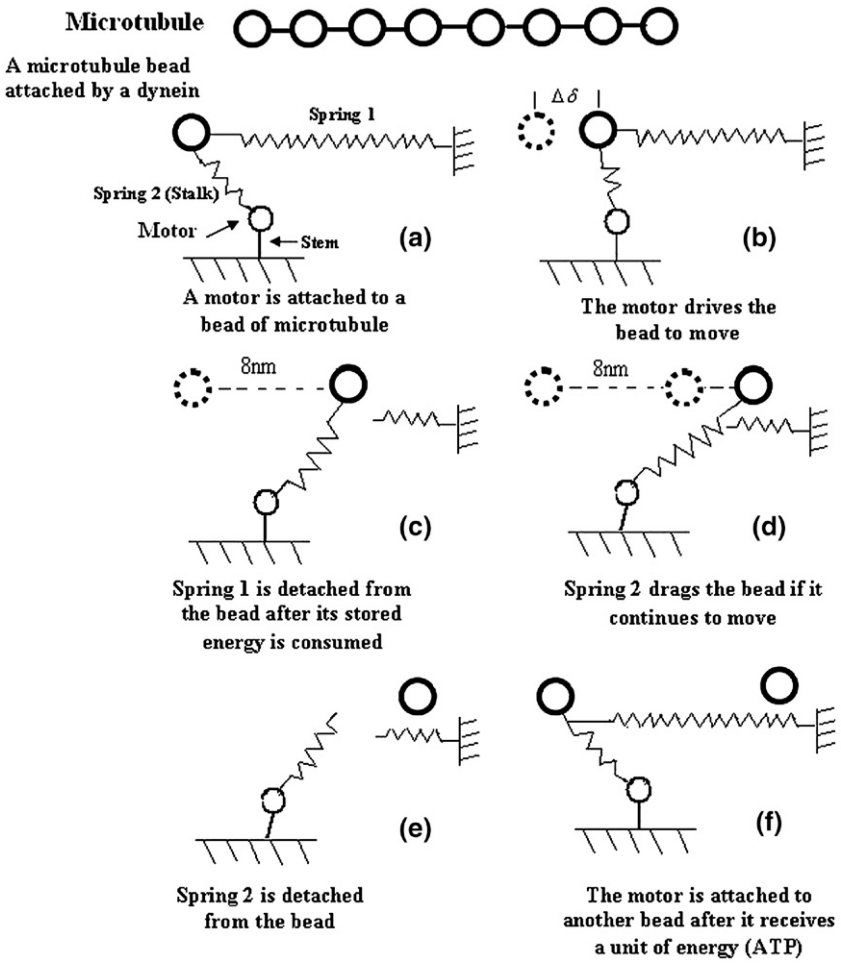

Fig. 3. The sketch of an attaching and detaching process.

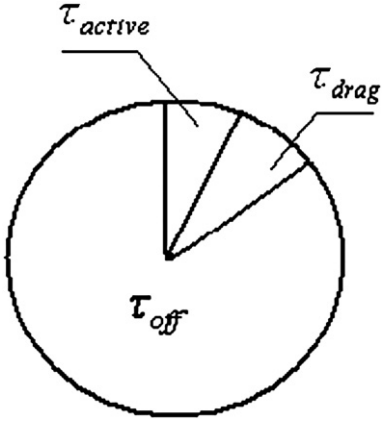

Fig. 4. An attaching and detaching cycle for dynein c.

In the model, two springs are used to represent the power stroke action as shown in Fig. 3: spring 1 is used to drive a microtubule to move forward, and spring 2, which represents the stalk of dynein, is used to capture the microtubule. The motor is attached to a glass surface by its stem, which is assumed to be rigid and can only wave around the fixed position. The stress-free length of the stalk is 15 nm and that of the stem is 13 nm. The diameter of motor is about 15 nm [11]. When a motor is attached to a microtubule, spring 1 is full of strain energy given by ATP hydrolysis and it drives the microtubule to move (the driving period is defined as τ_{active}). After the displacement (8 nm) is accomplished and the strain energy in spring 1 is consumed, spring 2 starts to drag the bead. As suggested [45], there exists a drag process by motor proteins; this is also logically expected, since the motor detachment may take some time that should not be ignored at the nano-scale. In the model, we assume that there is a short period (τ_{drag}) for a motor to be completely detached from a microtubule. During τ_{drag}, the motor drags the microtubule, since the latter still moves even there is a resistant force from the solution. During the following period of detachment (τ_{off}), the motor would obtain another energy unit from ATP hydrolysis and then grab the microtubule again, followed by another cycle, as Fig. 3 illustrates.

The total attachment period τ_{on} is the sum of τ_{active} and τ_{drag}, $\tau_{on}=\tau_{active}+\tau_{drag}$. The cycle period time of dynein c is about 10 ms. The duty ratio for dynein c is 0.14. Hence for dynein c, τ_{off} is about 6 times as long as τ_{on}.

In the model, the driving period (τ_{active}) of dynein c was assumed to be the same as τ_{drag}, which can, of course, be adjusted to match experimental observation. Such an assumption should not lead to misleading information when studying the mechanism for motor-microtubule interaction, rather than intending to obtain accurate quantitative data. Fig. 4 schematically illustrates the three periods of an attaching and detaching cycle for a dynein c.

3. Results and discussion

3.1. The effect of motor density on the microtubule motility

Since the attachment of protein motors onto a microtubule is statistically random, the coordination among protein motors should affect the motion of a microtubule driven by the motors. The coordination among protein motors is dependent on the number of protein motors, which can affect the driving and drag forces on the microtubule and thus its motion. In order to gain an insight into this issue, the movement of a microtubule driven by dynein c with different motor densities was simulated. The system for modeling was set as 200×40 as shown in Fig. 2. The length of a microtubule was set as 100, consisting of 100 beads. In order to study how the density of motor protein affected the microtubule's movement, different motor densities, which represent the number of dynein c motors per micrometer along the longitudinal direction of the system, were used in the simulation. Motors were randomly distributed in the longitudinal direction, along which the microtubule moved.

Fig. 5 illustrates the displacement of a microtubule along the longitudinal direction against time or time steps for different densities of dynein c. As shown, when the microtubule was driven by a motor, a stepwise-curve was observed. In this case, as the motor was attached to the microtubule, it drove the microtubule to move over one step (δ) with releasing its stored energy. The motor then dragged the microtubule before it was completely detached from the microtubule. As a result, the microtubule stopped to move due to the drag from both the motor and the surrounding liquid. After an off-attaching period τ_{off}, the motor was attached to the microtubule again (in another position) and another attaching–driving–detaching cycle began. This stepwise curve was observed experimentally, as

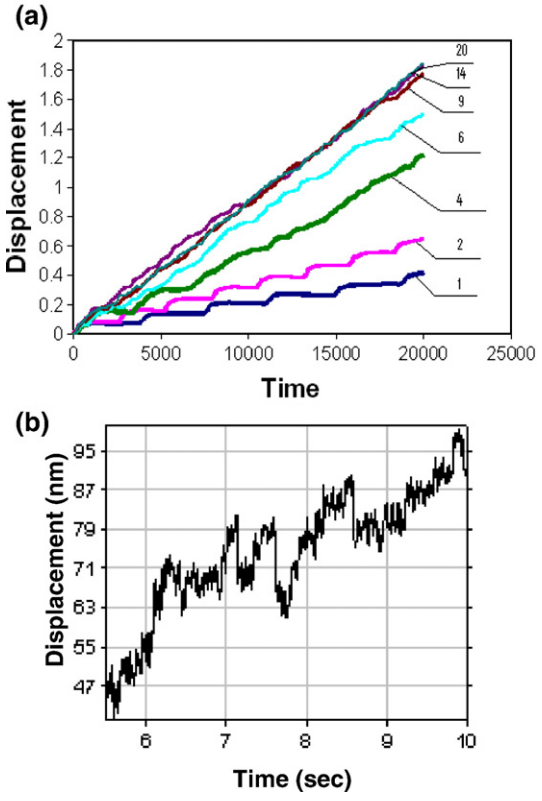

Fig. 5. (a) The simulated displacement of a microtubule vs. the time (different motor densities were used in the simulation, respectively); (b) Stepwise movement of a microtubule driven by a single dynein c [44].

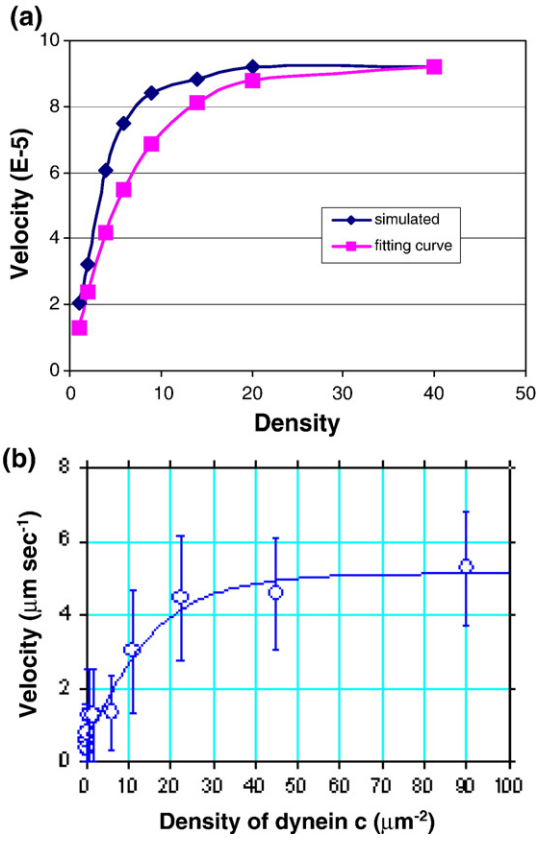

Fig. 6. (a) The velocity of microtubule vs the density of motors; (b) The sliding velocity of microtubule vs the surface density of dynein c [44].

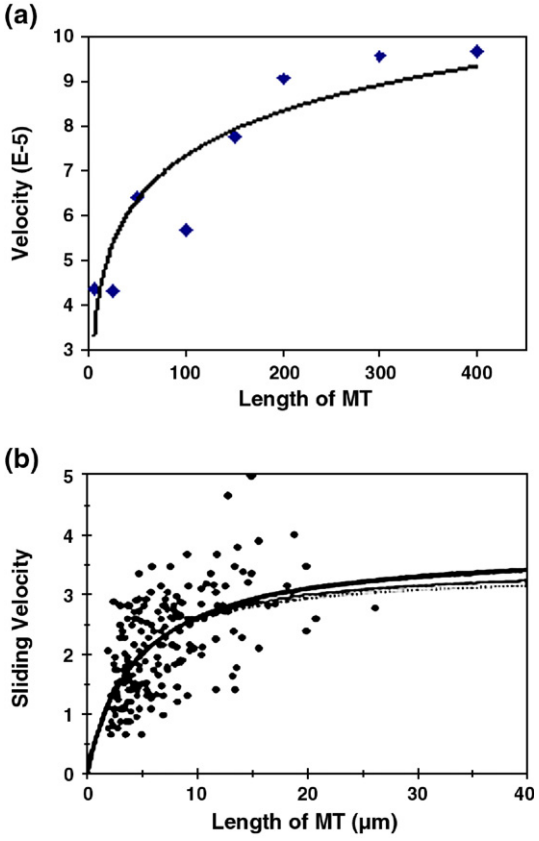

Fig. 7. (a) The simulated velocity of microtubule against its length (b) Experimentally observed sliding velocity of a microtubule against its length (cited from Ref [46]).

Fig. 5 (b) illustrates [44]. The experiential stepwise curve is not as regular as the one from simulation, since a realistic moving process on nano scale could be very sensitive to any disturbance from the surrounding medium under the experimental condition. The stepwise curve was also observed when more motors were involved; however, the curve became less stepwise. As shown in Fig. 5 (a), the movement of microtubule becomes continuous with an increase in the motor density and the displacement–time curve eventually turns into a line.

The velocity of microtubule increases as the density of dyneins (the number of dynein c motors per micrometer) increases, since the time interval during which the microtubule stops to move decreases as Fig. 5 (a) illustrates. As a result, the average velocity increases, i.e., the average slop of the curve increases. Fig. 6 (a) illustrates the increase in velocity against the motor density. As shown, the velocity increases rapidly with an increase in the density of molecular motors until saturation when the motor density reaches a certain level. The saturation of velocity may be largely attributed to an increase in the drag from the motors as the motor density increases, which renders the coordination among motors poor. A balance between driving and drag is eventually be reached, leading to a stable velocity as the motor density reaches a certain value, as Fig. 6 (a) illustrates.

The relation between the velocity V_s and motor density D may be approximately represented using the following equation: $V_s = V_{S0} * (1-(1-0.14)^D)$, where $V_{S0} = 9.225\text{E-}5$. Experimentally, a similar relationship was observed between the velocity and motor density: $V_{exp} = V_0(1-(1-f)^N)$, where f is the duty ratio = 0.14 for dynein c and N is proportional to the motor density [44]. Fig. 6 (b) illustrates the experimental result, which is consistent with the modeling result.

3.2. The length of microtubule and sliding velocity

Previous work demonstrated that the motility of microtubule was affected by its length [46], which should also be influenced by the coordination among protein motors. For a fixed motor

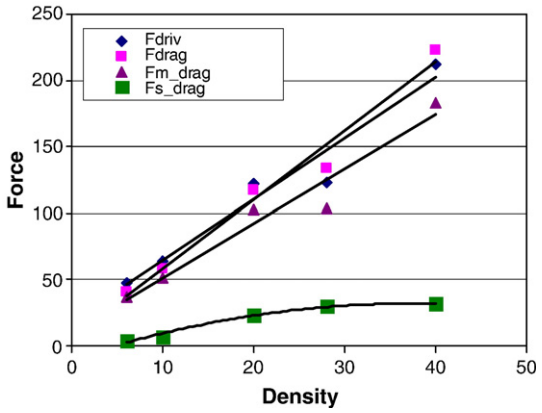

Fig. 8. F_{driv}, F_{drag}, F_{m_drag}, and F_{s_drag} vs. the density of dynein c motors.

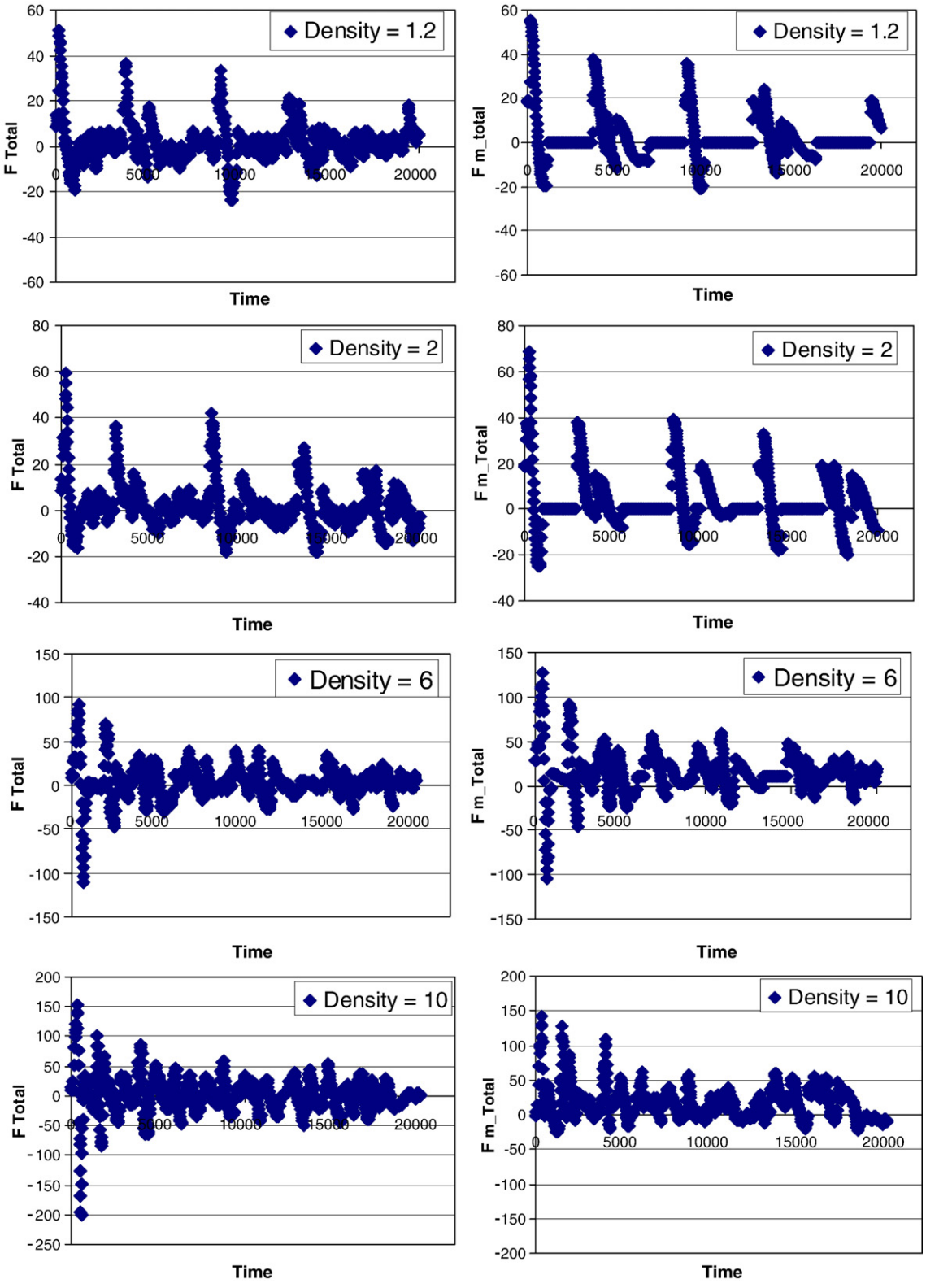

Fig. 9. Average F_{total} and F_{m_total} vs. the time steps for different motor densities.

density, the longer a microtubule, the lower degree should be the motor coordination. This consequently affects the microtubule's velocity. In order to elucidate the relation between the microtubule length and velocity, the motion of microtubules having different lengths driven by motors with the same density was simulated. In the model, the average density of motors was fixed as 10 dynein c motors per micrometer along the longitudinal moving direction. Motors were randomly distributed in the

system. In the model, microtubules having different lengths, 6, 12, 25, 50, 100, 150, 200, 300, and 400, respectively, were studied.

Fig. 7 (a) illustrates the longitudinal velocity of a microtubule against its length. The velocity increased initially with an increase in the length, which became stable after reaching a critical length. Similar trend was observed in reported experiments [46] as shown in Fig. 7 (b).

For a short microtubule, motors have a lower probability to attach and drive it. Hence, the microtubule should move slowly as the total driving force from motors becomes smaller. With an increase in the length of microtubule, more motors have the opportunity to attach and drive it with more local acceleration events associated with motor attachment, thus resulting in an increase in the velocity of microtubule. However, along with the increase in the driving force, the drag force from motors also increases, accompanied with poor motor coordination as indicated earlier. Meanwhile, the drag force from solution also increases due to the increased velocity and length of a microtubule. As a result, the velocity of microtubule eventually becomes saturated as the microtubule's length reaches a certain value.

3.3. Force analysis

As indicated earlier, a microtubule may exhibit very different kinetic behaviors when driven by a single motor and a group of motors, respectively. The higher the motor density, or the longer the microtubule, the more motors attached to the microtubule simultaneously. Therefore, understanding how motors work coordinately to drive microtubule is of importance to gain better understanding of the effect of motor density on microtubule's kinetic behavior, which is crucial to future nano-bio-mechanical systems. Obviously, the coordination of motors directly affects the driving and drag forces to a microtubule. In this study, we investigated the effects of the motor density on drag force (F_{drag}) and driving force (F_{driv}). There are two net drag forces: one from motors, $F_{\text{m\_drag}} = \sum_{i=1}^{N_0} F^i_{\text{m\_drag}}$ ($F^i_{\text{m\_drag}} \neq 0$ when the motor i is in its period of τ_{drag}) and the other from the interaction between the microtubule and solution particles, $F_{\text{s\_drag}} = \sum_{i=1}^{N_1} \sum_{j=1}^{N_2} F^{\text{D}}_{ij}$. N_0 is the total number of motors, N_1 is the number of beads within a microtubule, and N_2 is the number of solution particles. The driving force is the total force from all motors that are attached to the microtubule, $F_{\text{driv}} = F_{\text{m\_driv}} = \sum_{i=1}^{N_0} F^i_{\text{m\_driv}}$. $F^i_{\text{m\_drag}}$ and $F^i_{\text{m\_driv}}$ are the drag force and driving force from motor i. The total force (F_{total}) on microtubule is the sum of $F_{\text{m\_drag}} + F_{\text{s\_drag}} + F_{\text{driv}}$.

Fig. 8 illustrates average F_{driv}, F_{drag}, $F_{\text{m\_drag}}$, and $F_{\text{s\_drag}}$ with respect to the density of dynein c motors (the number of dynein c motors per micrometer). With an increase in the motor density, F_{driv}, F_{drag}, $F_{\text{m\_drag}}$, and $F_{\text{s\_drag}}$ increased. It is understandable that the first three forces are proportional to the motor density, since they are directly contributed by individual motors and affected by their coordination. Regarding the drag force from solution, although increased initially, it reached a stable value when the density exceeded 20. Since $F_{\text{s\_drag}}$ is related to the velocity of microtubule beads relative to solution particles, it is mainly influenced by the velocity of the microtubule. As demonstrated earlier, the velocity of microtubule increased initially with an increase in motor density, associated with a corresponding increase in drag force from solution. However, the velocity of microtubule became stable when the density exceeded 20 (see Fig. 6 (a)). Hence, $F_{\text{s\_drag}}$ should also become stable when the motor density exceeds this value as Fig. 8 illustrates.

Comparing to the drag force from solution ($F_{\text{s\_drag}}$), the drag force from motors ($F_{\text{m\_drag}}$), was larger. This implies that motors play important role in dragging the microtubule, so that the coordination among motors should have a strong influence on the drag action. When comparing the total drag force to the total driving force, though they both increased with an increase in the density of motors, one may see that the ratio of these two forces is close to 1. This may make the microtubule moves at a constant speed.

Fig. 9 illustrates F_{total} and $F_{\text{m\_total}}$ against the time step for different densities of dynein motor. As illustrated, the total force on microtubule fluctuated with time. With an increase in motor density, the fluctuation frequency increased. However, the average total force for a long period was zero. This indicates that statistically a microtubule moves at a constant average speed but acceleration exists once a motor is attached to the microtubule. Such acceleration becomes less visible with an increase in the motor density.

The total force from motors, $F_{\text{m\_total}}$, showed similar fluctuation but its average was non-zero, since the average force from motor should be non-zero in order to overcome the resistance from the solution as well as that from motor's drag when the microtubule is moving. The positive value corresponded to the driving force provided by the motor when it was attached to the microtubule, while the negative value corresponded to the drag force from the motor during the detaching period (τ_{drag}). The fluctuation frequency became higher as the motor density was increased, leading to more stable motion of the microtubule.

The effect of the coordination among motors and its influences on the driving and drag forces, average F_{driv}, F_{drag}, $F_{\text{m\_drag}}$, and $F_{\text{s\_drag}}$ against the length of microtubule were also investigated. As shown in Fig. 10, with an increase in the microtubule's length, F_{drag}, F_{driv}, and $F_{\text{m\_drag}}$ continuously increased. The increases in the forces are attributed to the fact that a longer microtubule can be attached by more motors that result

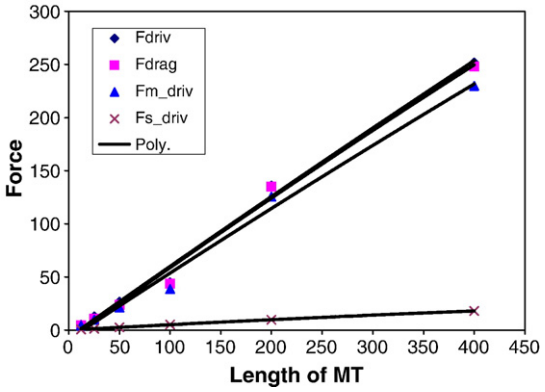

Fig. 10. The forces F_{driv}, F_{drag}, $F_{\text{m\_drag}}$, and $F_{\text{s\_drag}}$ vs. the length of microtubule.

in not only a larger average driving force but also a larger drag force due to inharmonic attachment by an increased number of motors. Besides, the resultant increase in microtubule's velocity also increased the drag force from solution.

In summary, the present modeling study has demonstrated effects of motor density and microtubule's length on the microtubule's velocity, driving and drag forces. The coordination of motors certainly has strong influences on these parameters, which have been qualitatively demonstrated in this modeling study. It should be pointed out that in the present study the authors do not attempt to establish quantitative relationships between the motor coordination and the kinetic behavior of a bio-filament driven by multiple protein motors. To do so, it is necessary to define an adequate statistical parameter to describe the motor coordination and further quantitative investigations and statistic analysis are needed.

4. Conclusion

A microscopic model based on the dissipative particle dynamic method and a bead-and-spring configuration was proposed to explore the driving mechanism for molecular motors attached to a microtubule. Effects of motor's density and the length of microtubule on the motion of a microtubule were studied, with the aim of demonstrating the influence of the coordination among protein motors on the motion of a microtubule.

It was demonstrated that with an increase in the motor's density, the average velocity of a microtubule increased and eventually became saturated. The microtubule's length showed a similar influence on the velocity. Detailed information on changes in the driving and drag forces with respect to the motor density and microtubule's length was obtained from the modeling study. The computational results are in agreement with experimental observations reported in literature. The observed phenomena are greatly related to the coordination among protein motors.

References

[1] N.J. Carter, R.A. Cross, Mechanics of the kinesin step, Nature 435 (2005) 308–312.
[2] J.J. Schmidt, C.D. Montemagno, Bionanomechanical systems, Annual Review of Materials Research 34 (2004) 315–337.
[3] H. Hess, G.D. Bachand, V. Vogel, Powering nanodevices with biomolecular motors, Chemistry—A European Journal 10 (2004) 2110–2116.
[4] M.E. Schliwa, Molecular Motors, Wiley-VCH, Weinheim, 2003.
[5] R.B. Vallee, P. Hook, Molecular motors: a magnificent machine, Nature 421 (2003) 701–702.
[6] H. Suzuki, K. Oiwa, A. Yamada, H. Sakakibara, H. Nakayama, S. Mashiko, Linear arrangement of motor protein on a mechanically deposited fluoropolymer thin-film, Japanese Journal of Applied Physics. Part 1, Regular Papers & Short Notes 34 (1995) 3937–3941.
[7] J.R. Dennis, J. Howard, V. Vogel, Molecular shuttles: directed motion of microtubules along nanoscale kinesin tracks, Nanotechnology 10 (1999) 232–236.
[8] H. Suzuki, A. Yamada, K. Oiwa, H. Nakayama, S. Mashiko, Control of actin moving trajectory by patterned poly(methyl methacrylate) tracks, Biophysical Journal 72 (1997) 1997–2001.
[9] Y. Hiratsuka, T. Tada, L. Oiwa, T. Kanayama, T.Q. Uyeda, Controlling the direction of kinesin-driven microtubule movements along microlithographic tracks, Biophysical Journal 81 (2001) 1555–1561.
[10] J. Clemmens, H. Hess, J. Howard, V. Vogel, Analysis of microtubule guidance in open microfabricated channels coated with the motor protein kinesin, Langmuir 19 (2003) 1738–1744.
[11] J. Clemmens, H. Hess, R. Lipscomb, Y. Hanein, K.F. Bohringer, C.M. Matzke, G.D. Bachand, B.C. Bunker, V. Vogel, Mechanisms of microtubule guiding on microfabricated kinesin-coated surfaces: chemical and topographic surface patterns, Langmuir 19 (2003) 10967–10974.
[12] C. Shingyoji, H. Higuchi, M. Yoshimura, E. Katayama, T. Yanagida, Dynein arms are oscillating force generators, Nature 393 (1998) 711–714.
[13] I. Rayment, W.R. Rypniewski, K. Schmidt-Base, R. Smith, D.R. Tomchick, M.M Benning, D.A. Winkelmann, G. Wesenberg, H.M. Holden, Three-dimensional structure of myosin subfragment-1: a molecular motor, Science 261 (1993) 50–58.
[14] F.J. Kull, E.P. Sablin, R. Lau, R.J. Fletterick, R.D. Vale, Crystal structure of the kinesin motor domain reveals a structural similarity to myosin, Nature 380 (1996) 550–555.
[15] S.A. Burgess, M.L. Walker, H. Sakakibara, P.J. Knight, K. Oiwa, Dynein structure and power stroke, Nature 421 (2003) 715–718.
[16] F. Gittes, B. Mickey, J. Nettleton, J. Howard, Flexural rigidity of microtubules and actin filaments measured from thermal fluctuations in shape, Journal of Cell Biology 120 (1993) 923–934.
[17] H. Nagashima, S. Asakura, Dark-field light microscopic study of the flexibility of F-actin complexes, Journal of Molecular Biology 136 (1980) 169–182.
[18] H. Kojima, A. Ishijima, T. Yanagida, Direct measurement of stiffness of single actin filaments with and without tropomyosin by in vitro nanomanipulation, Proceedings of the National Academy of Sciences of the United States of America 91 (1994) 12962–12966.
[19] R. Yasuda, H. Miyata, K. Kinosita Jr., Direct measurement of the torsional rigidity of single actin filaments, Journal of Molecular Biology 263 (1996) 227–236.
[20] M.P. Sheetz, J.A. Spudich, Movement of myosin-coated fluorescent beads on actin cables in vitro, Nature 303 (1985) 31–35.
[21] J. Howard, A.J. Hudspeth, R.D. Vale, Movement of microtubules by single kinesin molecules, Nature 342 (1989) 154–158.
[22] M.B. Viani, L.I. Pietrasanta, J.B. Thompson, A. Chand, I.C. Gebeshuber, J.H. Kindt, M. Richter, H.G. Hansma, P.K. Hansma, Probing protein–protein interactions in real time, Nature Structural Biology 7 (2000) 644–647.
[23] H. Kojima, M. Kikumoto, H. Sakakibara, K. Oiwa, Mechanical properties of a single-headed processive motor, inner-arm dynein subspecies-c of *Chlamydomonas* studied at the single molecule level, Journal of Biological Physics 28 (2002) 335–345.
[24] T. Wazawa, M. Ueda, Total internal reflection fluorescence microscopy in single molecule nanobioscience, Microscopy Techniques Advances in Biochemical Engineering/Biotechnology 95 (2005) 77–106.
[25] A.F. Huxley, Muscle structure and theories of contraction, Progress in Biophysics and Molecular Biology 7 (1957) 255–318.
[26] K.C. Holmes, The swinging lever-arm hypothesis of muscle contraction, Current Biology 7 (1997) R112–R118.
[27] R.D. Astumian, M. Bier, Fluctuation driven ratchets: molecular motors, Physical Review Letters 72 (1994) 1766–1769.
[28] J. Howard, The movement of kinesin along microtubules, Annual Review of Physiology 58 (1996) 703–729.
[29] C.L. Asbury, A.N. Fehr, S.M. Block, Kinesin moves by an asymmetric hand-over-hand mechanism, Science 302 (2003) 2130–2134.
[30] H. Qian, A simple theory of motor protein kinetics and energetics, Biophysical Chemistry 67 (1997) 263–267.
[31] Y.Q. Gao, W. Yang, R.A. Marcus, M. Karplus, A model for the cooperative free energy transduction and kinetics of ATP hydrolysis by F1-ATPase, Proceedings of the National Academy of Sciences of the United States of America 100 (2003) 11339–11344.
[32] P.J. Hoogerbrugge, J.M.V.A. Koelman, Simulation microscopic hydrodynamic phenomena with dissipative particle dynamics, Europhysics Letters 19 (1992) 155–160.
[33] J.M.V.A. Koelman, P.J. Hoogerbrugge, Dynamic simulation of hard-sphere suspensions under steady shear, Europhysics Letters 21 (1993) 363–368.
[34] A.G. Schlijper, P.J. Hoogerbrugge, C.W. Manke, Computer simulation of dilute polymer solutions with the dissipative particle dynamics method, Journal of Rheology 39 (1995) 567–579.

[35] Y. Kong, C.W. Manke, W.G. Madden, Effect of solvent quality on the conformation and relaxation of polymers via dissipative particle dynamics, Journal of Chemical Physics 107 (1997) 592–602.
[36] J.B. Gibson, K. Chen, S. Chynoweth, Simulation of particle adsorption onto a polymer-coated surface using the dissipative particle dynamics method, Journal of Colloid and Interface Science 206 (1998) 464–474.
[37] C.M. Wijmans, B. Smit, R.D. Groot, Phase behavior of monomeric mixtures and polymer solutions with soft interaction potentials, Journal of Chemical Physics 114 (2001) 7644–7654.
[38] T. Soddemann, B. Dünweg, K. Kremer, Dissipative particle dynamics: a useful thermostat for equilibrium and nonequilibrium molecular dynamics simulations, Physical Review. E, Statistical Physics, Plasmas, Fluids, and Related Interdisciplinary Topics 68 (2003) 046702-2.
[39] A. Satoh, T. Majima, Comparison between theoretical values and simulation results of viscosity for the dissipative particle dynamics method, Journal of Colloid and Interface Science 283 (2005) 251–266.
[40] B.R.B.C.F. Curtiss, R.C. Armstrong, O. Hassager, Dynamics of Polymeric Liquids, Wiley, New York, 1987.
[41] M.P. Allen, D.J. Tildesley, Computer Simulation of Liquids, Oxford University Press, New York, 1987.
[42] L. Amos, A. Klug, Arrangement of subunits on flagellar microtubules, Journal of Cell Science 14 (1974) 523–549.
[43] R.D. Groot, P.B. Warren, Dissipative particle dynamics: bridging the gap between atomistic and mesoscopic simulation, Journal of Chemical Physics 107 (1997) 4423–4435.
[44] H. Sakakibara, H. Kojima, Y. Sakai, E. Katayama, K. Oiwa, Inner-arm dynein c of *Chlamydomonas* flagella is a single-headed processive motor, Nature 400 (1999) 586–591.
[45] J. Howard, Mechanics of motor proteins and the cytoskeleton, Sinauer Associates, Inc., Sunderland, Massachusetts, 2001.
[46] T. Hamasaki, M.E.J. Holwill, K. Barkalow, P. Satir, Mechanochemical aspects of axonemal dynein activity studied by in vitro microtubule translocation, Biophysical Journal 69 (1995) 2569–2579.